Exploration of Charge Storage Behavior of Binder-Free EDL Capacitors in Aqueous Electrolytes

Bhupender Pal,* Kalyan Jyoti Sarkar, Bing Wu, Lukáš Děkanovský, Vlastimil Mazánek, Rajan Jose, and Zdeněk Sofer*

ACCESS | Metrics & More | Article Recommendations | Supporting Information

ABSTRACT: Charge storage in electrochemical double-layer capacitors (EDLCs) is via the adsorption of electrolyte counterions in their positive and negative electrodes under an applied potential. This study investigates the EDLC-type charge storage in carbon nanotubes (CNT) electrodes in aqueous acidic ($NaHSO_4$), basic (NaOH), and neutral (Na_2SO_4) electrolytes of similar cations but different anions as well as similar anions but different cations (Na_2SO_4 and Li_2SO_4) in a two-electrode Swagelok-type cell configuration. The physicochemical properties of ions, such as mobility/diffusion and solvation, are correlated with the charge storage parameters. The neutral electrolytes offer superior charge storage over the acidic and basic counterparts. Among the studied ions, SO_4^{2-} and Li^+ showed the most significant capacitance owing to their larger solvated ion size. The charge stored by the anions and cations follows the order $SO_4^{2-} > HSO_4^- > OH^-$ and $Li^+ > Na^+$, respectively. Consequently, the $CNT//Li_2SO_4//CNT$ cell displayed outstanding charge storage indicators (operating voltage $\sim0-2$ V, specific capacitance ~122 F·g^{-1}, specific energy ~67 W h·kg^{-1}, and specific power ~541 W·kg^{-1} at 0.5 A·g^{-1}) than the other cells, which could light a red light-emitting diode (2.1 V) for several minutes. Besides, the $CNT//Li_2SO_4//CNT$ device showed exceptional rate performance with a capacitance retention of $\sim95\%$ at various current densities (0.5−2.5 A·g^{-1}) after 6500 cycles. The insights from this work could be used to design safer electrochemical capacitors of high energy density and power density.
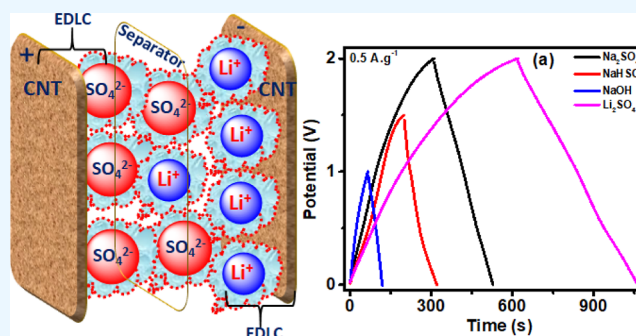
1. INTRODUCTION

Electrochemical energy storage systems are considered as eco-friendly energy technologies concerning a clean atmosphere and environment. In an electrochemical energy storage system, we can use chemical energy to provide electrical energy as per our needs without any environmental pollution.[1−3] In these conditions, electrochemical capacitors have captivated the energy storage technology due to their excellent life cycle stability and higher power density compared to electrochemical batteries.[4,5] Electrochemical capacitors based on activated carbon as electrode materials have been commercialized due to their high specific surface area, long life cycle stability, and low cost, although activated carbon suffers from its low electrical conductivity.[6−9] Therefore, electrode materials based on carbon nanotubes (CNTs) (cylindrical graphitic structure contributes to high electron mobility) will be suitable for next-generation electrochemical capacitors due to their higher electrical conductivity than activated carbon.[10] The mechanical strength of CNTs is very high (Young's modulus ~34 GPa), and the electrodes based on CNTs also suppress the volume change upon cycling.[10] Likewise, electrochemical capacitor's energy density ($E = 1/2CV^2$) is directly proportional to its specific capacitance and the square

of the operational voltage window.[3] The stability of the operational voltage window depends on the electrochemical properties of the electrolyte; consequently, optimizing electrolytes is an effective way to harvest high energy density-based electrochemical capacitors.

Additionally, electrolytes help in balancing and transferring charges between two electrodes; therefore, they play a very significant and crucial role in electrochemical capacitors.[3,11,12] The internal structure of electrode materials and the state of electrode−electrolyte interface are significantly affected by the interaction between the electrode and electrolyte during electrochemical processes.[13] Therefore, the choice of the electrolyte is very crucial for the safety and high performance of electrochemical capacitors. On the other hand, the performance of electrochemical capacitors is decided not only by the exposed surface of the electrode materials but also

Table 1. Electrochemical Performance of Some CNT-Based Electrochemical Capacitors (Full Device)

electrolytes	electrodes	specific capacitance (F·g^{-1})	energy density (W h·kg^{-1})	power density (kW·kg^{-1})	cell voltage (V)	refs
1 M H$_2$SO$_4$ aqueous	MWCNT film on PET (CNT//CNT)	39 (20 mV·s^{-1})	0.02	58	1	28
LiClO$_4$/EC:DEC:DMC	CNT film (CNT//CNT)	35	43.7	197.3	3	29
1 M TEABF$_4$/PC organic	CNT film (CNT//CNT)	23 (100 A·g^{-1})	4.2	55	1.5	30
LiPF$_6$/EC:DMC:EMC	CNT film (CNT//CNT)	28.5			2	31
1 M Et$_4$NBF$_4$/PC organic	DWCNT/TWCNT and long MWCNT (CNT//CNT)	59.1 F (10 mV·s^{-1})	35	3	4	32
TBAPF$_6$/PMMA/PC/ACN	SWCNT film on PDMS (CNT//CNT)	34.2 (0.63 A·g^{-1})	18	21.1	2	33
PVA/H$_3$PO$_4$ and LiPF$_6$/EC:DEC	printed SWCNT film on PET (CNT//CNT)	120	6	23 and 70	1 and 3	34
1 M TEABF$_4$/PC organic	CNT film on PDMS (CNT//CNT)	54	5.2	3−4	1.5	35
PVA/H$_2$SO$_4$ aqueous gel	CNT film on PDMS (CNT//CNT)	53		32	0.8	36
1 M TEABF$_4$/PC organic	CNT film on PDMS (CNT//CNT)	44			1.5	37
LiClO$_4$/EC:DEC:DMC	CNT film on PET (CNT//CNT)	22.5	12.5	13.9	2.0	38
PVDF-HFP/EMIMTFSI	sprayed SWCNT film on metal coated PDMS (CNT//CNT)	51.8	15.7	1.48	3	39
6 M KOH	N-doped CNTs	336	17.2	300	1.2	40
PVA-H$_3$PO$_4$	N,S-doped CNTs	195.2			0.8	41
EhNBF$_4$/PC	N−C nanotube	252	30	625	2.5	42
1 M NaHSO$_4$ aqueous	CNT//CNT	~41 (at 0.5 A·g^{-1})	~13	~3.7	1.5	this work
1 M Na$_2$SO$_4$ aqueous	CNT//CNT	~56 (at 0.5 A·g^{-1})	~31	~5	2	this work
1 M NaOH aqueous	CNT//CNT	~27 (at 0.5 A·g^{-1})	~4	~2.6	1	this work
1 M Li$_2$SO$_4$	CNT//CNT	~122 (at 0.5 A·g^{-1})	~67	~541	2	this work

by the matching degree between the pore size distribution of the carbon electrode and the size of solvated ions in the electrolyte.[14,15] Various research groups have studied the electrolytes for an electrochemical double-layer capacitor (EDLC) system in numerous application conditions.[16−18] Aqueous and non-aqueous electrolytes are two major types of electrolytes in the EDLC system.[14,19−21] Non-aqueous electrolytes (such as organic and ionic liquids) have been used in commercial electrochemical capacitors due to their high operational voltage window.[22] However, they have low charge storage capacity and cycle stability due to their low ionic conductivity, large molecule radius, and high viscosity.[22,23] Moreover, their competitiveness is also weak due to their safety (volatility and inflammability) and high cost. On the other hand, aqueous electrolytes have low viscosity, high ionic conductivity, and small ionic radius, which further help them to improve the power capability and cycle stability of an electrochemical capacitor.[23] The charge storage performances of some CNT-based electrochemical capacitors are shown in Table 1.

Carbon-based electrochemical capacitors and various aqueous electrolytes[24,25] have been studied with same anions[26] but with different cations.[27] However, to the best of our knowledge, the effects of aqueous electrolytes (same cations with different anions and same anions with different cations) on CNT-based electrochemical capacitors have not been studied. This study investigates difference in the EDLC-type charge storage process in CNT electrodes in aqueous acidic (NaHSO$_4$), basic (NaOH), and neutral (Na$_2$SO$_4$) electrolytes of similar cations but different anions as well as similar anions but different cations (Na$_2$SO$_4$ and Li$_2$SO$_4$) in a two-electrode Swagelok-type cell configuration. In addition, because of the diverse range of electrode materials and potential window quantification criteria, a direct comparison between reports in

the literature is not feasible. For meaningful comparisons, it is necessary to study the effect of various anions with the same cation on the specific energy of EDLCs made of the same electrode materials (CNTs) and characterized with the same potential window quantification method. The objective of the current work is to understand the electrochemical behavior of the four different types of aqueous electrolytes (acidic, neutral, and basic) in the presence of microporous CNTs as a model system because of the uniformity, porosity, and high degree of interconnectedness of their mesopores. The CNT//Li$_2$SO$_4$//CNT device (0−2 V) showed an exceptional rate performance with a capacitance retention of ~96% at various current densities (0.5−2.5 A·g^{-1}) after 6500 cycles. The CNT//Li$_2$SO$_4$//CNT device was also able to light up a red light-emitting diode (LED, 2.1 V) for more than 2 min.

2. EXPERIMENTAL DETAILS

2.1. Materials Preparation and Characterization. Sodium hydroxide (NaOH), sodium sulfate (Na$_2$SO$_4$), lithium sulfate (Li$_2$SO$_4$), and sodium bisulfate (NaHSO$_4$) were purchased from Penta, Czech Republic, and TUBALL CNTs were provided by OCSiAl, Germany. The chemicals and reagents were used as such without further purification. First, 3 g of SWCNTs was dispersed in concentrated H$_2$SO$_4$ (600 mL, 96 wt %) by mechanical stirring (300 rpm), and 0.5 g of KMnO$_4$ was added in five portions over 30 min. The above reaction mixture was stirred at room temperature for 3 h before being purged in 5 L of deionized water. Oxidized SWCNTs were decanted three times, then separated by suction filtering, rinsed with deionized water three times, and washed with ethanol three times before being baked in a vacuum oven at room temperature for 50 h. Using an Ultraturrax T18 dispersing equipment, the separated SWCNTs
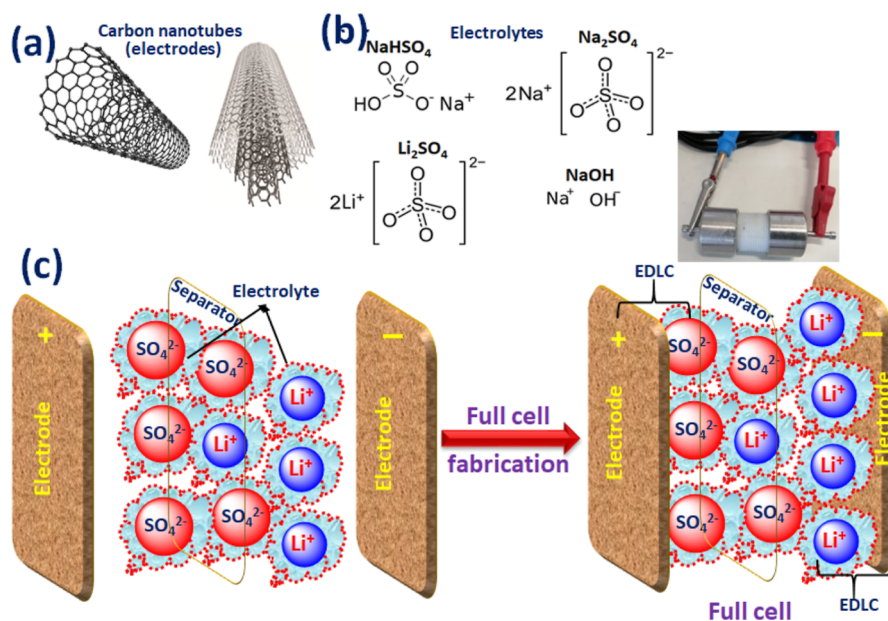
Figure 1. (a) Structure of CNTs; (b) structure of anions and cations of electrolytes (NaHSO$_4$, Na$_2$SO$_4$, Li$_2$SO$_4$, and NaOH) investigated in this study; and (c) schematic illustration of fabrication of symmetric electrochemical capacitors.
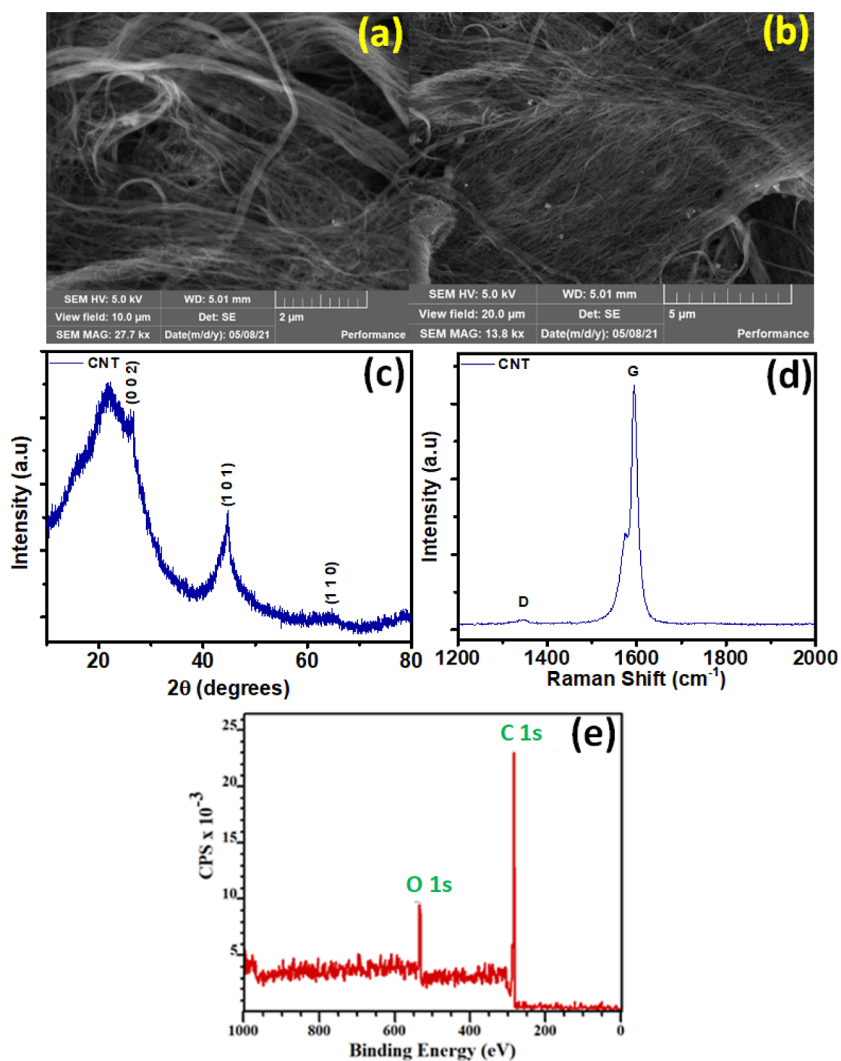

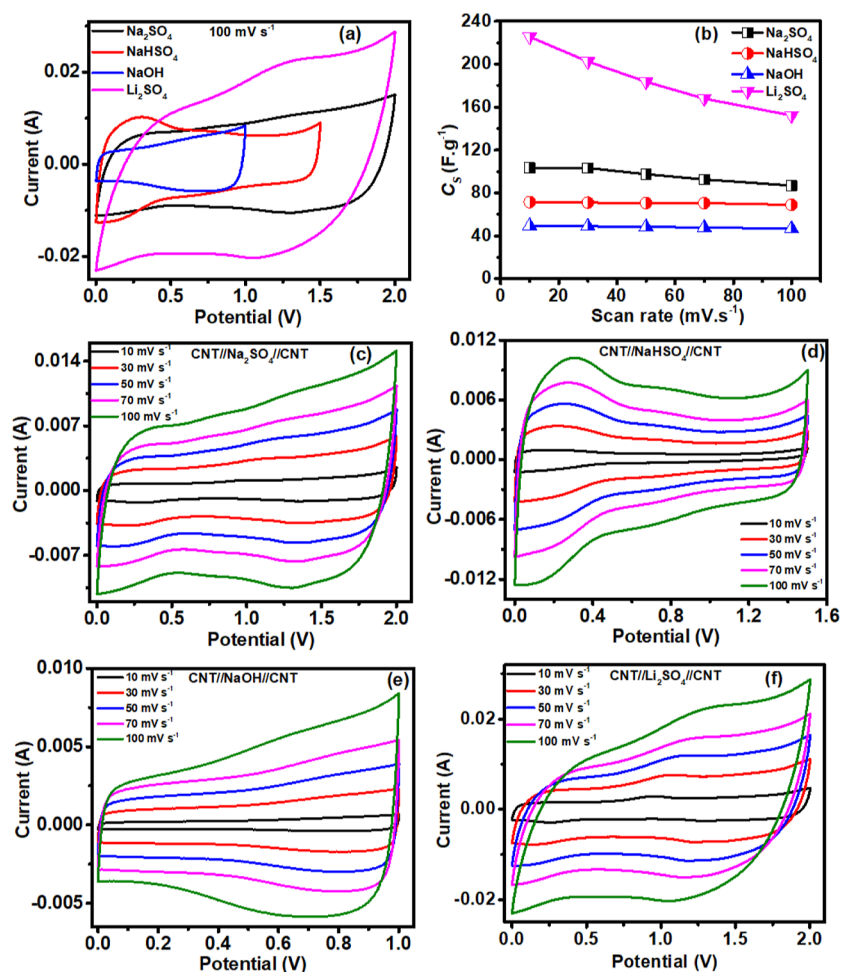**Figure 2.** (a,b) SEM images, (c) XRD pattern, (d) Raman, and (e) XPS spectra of CNTs.

Figure 3. (a) Comparison of cyclic voltammograms of CNT//Na$_2$SO$_4$//CNT, CNT//NaHSO$_4$//CNT, and CNT//NaOH//CNT full devices at 100 mV·s^{-1}. (b) Calculated C_S for CNT//Na$_2$SO$_4$//CNT, CNT//NaHSO$_4$//CNT, CNT//NaOH//CNT, and CNT//Li$_2$SO$_4$//CNT full devices at various scan rates. (c−f) CV graphs of CNT//Na$_2$SO$_4$//CNT, CNT//NaHSO$_4$//CNT, CNT//NaOH//CNT, and CNT//Li$_2$SO$_4$//CNT full devices at various scan rates.

were dispersed in deionized water (2.5 g/L) for 1 h at a speed of 12,000 rpm. Four different types of aqueous electrolytes including acidic, basic, and neutral were prepared by using NaHSO$_4$, NaOH, Na$_2$SO$_4$, and Li$_2$SO$_4$ salts as the solute and deionized water as the solvent. A 1 M concentration of each electrolyte has been prepared and used to make a complete device with CNTs as the electrode material. The morphology of CNTs was investigated using a scanning electron microscope (Tescan MAIA 3) equipped with an energy-dispersive spectrometer (Oxford Instruments, England). The X-ray diffractometer (Bruker D8 with Cu Kα radiation, Germany) was used to determine the crystal structure of CNTs. Raman spectroscopy (using a 532 nm laser, Renishaw, England) and X-ray photoelectron spectroscopy (XPS, SPECS, Germany) were used to identify the vibrational mode and surface composition. The Brunauer−Emmett−Teller (BET) surface area analyzer was used to examine the specific surface area, pore volume, and pore size of the samples.

2.2. Device Fabrication. The fabrication of the CNT// aqueous electrolyte//CNT device is shown graphically in Figure 1c. For the CNT electrodes, the symmetric electrochemical capacitors were fabricated without the use of any conductivity agent (Super P), binder, ionic solvent (NMP), and so forth. In a two-electrode setup with a Teflon Swagelok-

type cell, the electrochemical performance of the CNT electrodes was evaluated. To ensure appropriate ion soaking, the CNT film was cut into 1 × 1 cm^2 pieces (mass = 1.5 mg per electrode) and immersed in aqueous electrolytes for 5−10 min. After 10 min, the electrodes were removed from the electrolyte solution and mounted in a Teflon Swagelok-type cell to fabricate the CNTs//aqueous electrolyte//CNTs device. The electrochemical characterization of a two-electrode system was studied using an Autolab PGSTAT204 (Eco Chemie, Utrecht, The Netherlands). The electrochemical characterization was performed at room temperature using electrochemical impedance spectroscopy (EIS), galvanostatic charge−discharge (GCD), and cyclic voltammetry (CV). CV and GCD were performed in a potential operational window ranging from 0 to 2 V at different scan rates (10−100 mV·s^{-1}) and current densities (0.35−2.5 A·g^{-1}). EIS measurements were recorded using an open-circuit potential at 10 mV in the frequency range of 10 mHz to 100 kHz.

3. RESULTS AND DISCUSSION

3.1. Morphological, Structural, and Compositional Analysis of CNTs. Figure 2a,b shows the scanning electron microscopy (SEM) images of CNTs. The surface of the CNTs shows a rough morphology at lower magnification, consisting

of long hair, very dense, and fiber-like structures that are irregularly packed with one another. Higher magnification images, on the other hand, showed that the surface comprises a network of interconnecting fibers with a porous structure, densely packed together in a weave-like orientation. The porous structure of the CNTs can further help in improving the ion storage and diffusion. Figure 2c shows the powder X-ray diffraction (XRD) patterns of CNTs. At 2θ = ~24°, a broad and asymmetric (0 0 2) diffraction peak corresponding to amorphous carbon was observed. Despite the presence of amorphous carbon in the CNTs, the crystallinity of the SWCNTs was demonstrated by the increased intensity of the (1 0 1) diffraction plane at 2θ = ~44.5°, which reflected the atomic structure of the rolled-up graphene sheets. Further evidence of the crystallinity of the SWCNT samples was revealed by the presence of peaks at 2θ = ~63.8 and ~77.9°, which was associated with the (1 1 0) and (1 1 0) planes. The Raman spectra of CNTs are shown in Figure 2d. The spectra exhibit a very sharp peak in the G band at 1578 cm^{-1} and a smaller peak in the D band at 1348 cm^{-1} that corresponds to carbonaceous materials. The D band (1348 cm^{-1}) results from the sp^3 vibrations of disordered and defected carbon atoms, whereas the G band (1578 cm^{-1}) results from the sp^2 vibration of carbon atoms in a 2D hexagonal lattice.[43] The graphitization of the carbon matrix was revealed by the sharp and narrow G band (full width at half-maximum 15.5 cm^{-1}) as expected for SWCNTs. The intensity ratio of G and D bands identifies the ratio of sp^2 and sp^3 carbon atoms, which also provides information about the degree of disordered domains in CNTs. As a result, the defect density ratio of the CNTs is decreased (I_G/I_D = 0.046). The defect density ratio values are much below unity, indicating that the matrix has a high graphitization level. The XPS examination provided additional confirmation of the constitutional elemental composition and bonding states. The XPS full survey spectrum of CNTs (Figure 2e) revealed an oxygen content of 13.69% and a carbon content of 86.31%. Figure S1a displays the high-resolution deconvoluted XPS spectra of C 1s and O 1s of CNTs, which further identify the current functional groups. Figure S1a illustrates the C 1s peaks for CNTs, which are designated as C=C, C−OH, C=O, and O=C−OH at 284.16, 284.77, 286.49, and 287.81 eV, respectively.[44] Figure S1b illustrates the O 1s peaks for CNTs as O=C and O−C at 533.73 and 532.47 eV, respectively. The BET surface area of CNTs was examined under a nitrogen atmosphere, which was confirmed as ~478 m^2/g with a pore volume and an average pore size of 1.46 mL/g and 4.87 nm, respectively (Figure S2a,b). The increased surface area results from the porous interconnect morphology of highly dense fiber and long hair-like assemblies that are arbitrarily overflowing with each other.

3.2. Electrochemical Measurements. The electrochemical properties of CNT//aqueous electrolytes//CNT devices were investigated at various current densities, operational voltages, and scan rates by assembling two-electrode symmetric cells. Furthermore, to verify the broad applicability of the CNT//aqueous electrolytes//CNT device, the red (2.1 V) LED was lighted up only by neutral electrolytes (CNT//Li$_2$SO$_4$//CNT). The CNT//Li$_2$SO$_4$//CNT device has shown an excellent electrochemical performance than CNT//Na$_2$SO$_4$//CNT, CNT//NaHSO$_4$//CNT, and CNT//NaOH//CNT devices. Figure 3a shows the comparison of CV curves for CNT//Na$_2$SO$_4$//CNT, CNT//NaHSO$_4$//CNT, CNT//NaOH//CNT, and CNT//Li$_2$SO$_4$//CNT full

devices at a scan rate of 100 mV·s^{-1}. An EDLC behavior of all devices is shown by the rectangular shape of CV graphs. The CNT//Li$_2$SO$_4$//CNT device has shown a higher area under the CV curve than CNT//Na$_2$SO$_4$//CNT, CNT//NaHSO$_4$//CNT, and CNT//NaOH//CNT devices, which evidently specifies an enhancement in charge storage. The CNT//Li$_2$SO$_4$//CNT and CNT//Na$_2$SO$_4$//CNT devices have displayed a wide voltage window (0−2 V), which further improves their electrochemical properties. Specifically, the CNT//Li$_2$SO$_4$//CNT device displayed a higher specific capacitance (C_S ~ 225 F·g^{-1}) at a scan rate of 10 mV·s^{-1} in comparison to C_S ~ 103 F·g^{-1} for CNT//Na$_2$SO$_4$//CNT, C_S ~ 71.5 F·g^{-1} for CNT//NaHSO$_4$//CNT, and C_S ~ 49.5 F·g^{-1} for CNT//NaOH//CNT devices at the same scan rate. Furthermore, the porous CNTs also assist in easy ion diffusion and offer more space for ion storage. From Figure 3b and Table S1, it can be seen that the C_S value decreases with the increase in scan rates for all the devices. Figure 3f shows the CV profile of the CNT//Li$_2$SO$_4$//CNT device at various scan rates (10−100 mV/s). It is noticeable that even at a higher scan rate, the CNT//Li$_2$SO$_4$//CNT device maintains its rectangular shape of the CV curve, which indicates an excellent stability of this device even at higher scan rates. The CV curves at various scan rates for CNT//Na$_2$SO$_4$//CNT, CNT//NaHSO$_4$//CNT, and CNT//NaOH//CNT devices are displayed in Figure 3c−e, respectively.

All the electrolytes (acidic, basic, and neutral) completely dissociate in water into the cations (Na$^+$ and Li$^+$) and anions (HSO$_4^-$, OH$^-$, and SO$_4^{2-}$) as shown in Figure 1b. The ionic mobility, ionic radius, hydrated ionic radius, and molar ionic conductivity of the electrolyte ions in an aqueous solution are shown in Table 2. The physical properties such as solvation

Table 2. Ionic Mobility, Molar Ionic Conductivity, Ionic Radius, and Hydrated Ionic Radius of the Electrolyte Ions in an Aqueous Solution at 298 K[25,45]

ion	ionic radius (Å)	hydrated sphere radius (Å)	ionic mobility (10^{-8} m^2 s^{-1} V^{-1})	molar ionic conductivity (mS m^2 mol^{-1})
Na$^+$	1.02	3.58	5.19	5.01
Li$^+$	0.60	3.82	4.01	3.86
HSO$_4^-$	1.84	2.21	5.18	5.00
SO$_4^{2-}$	2.58	3.79	8.29	16.00
OH$^-$	1.33	3.00	20.64	19.91

energies, diffusion coefficient, and solvent−solvent, ion−solvent, and ion−ion interactions are also significant because they directly influence the operational voltage window, capacitance, and charge propagation of an electrochemical cell. Neutral electrolyte (CNT//Li$_2$SO$_4$//CNT and CNT//Na$_2$SO$_4$//CNT)-based devices displayed a higher potential window (2 V) than acidic (NaHSO$_4$, 1.5 V) and alkaline (NaOH, 1 V) electrolytes. The reason behind the higher potential window for neutral electrolytes is the very low concentration of OH$^-$ and H$^+$ ions which further decrease the hydrogen and oxygen evolution.[12] Thus, the potential window is in the following order: Li$_2$SO$_4$ = Na$_2$SO$_4$ > NaHSO$_4$ > NaOH. The mechanism for cation and anion charging/discharging processes is displayed in Figure 4a−d. The electrochemical capacitors showed remarkable changes in capacitance and current response only by changing the anions and cations of electrolytes that may be due to the difference in the physical properties of electrolytes, as shown in Table 2.
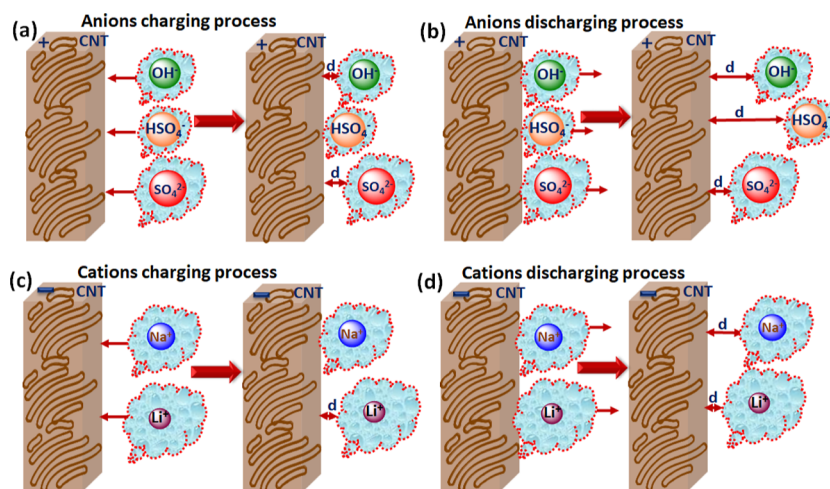
Figure 4. Schematic illustration of mobility of various anions and cations (hydrated ions) from an electrolyte medium to CNT electrodes at the time of charging and discharging processes. (a−d) CNT//Na$_2$SO$_4$//CNT, CNT//NaHSO$_4$//CNT, CNT//NaOH//CNT, and CNT//Li$_2$SO$_4$//CNT full devices; the mobility of hydrated ions depends on their hydrated sphere radius (Å).
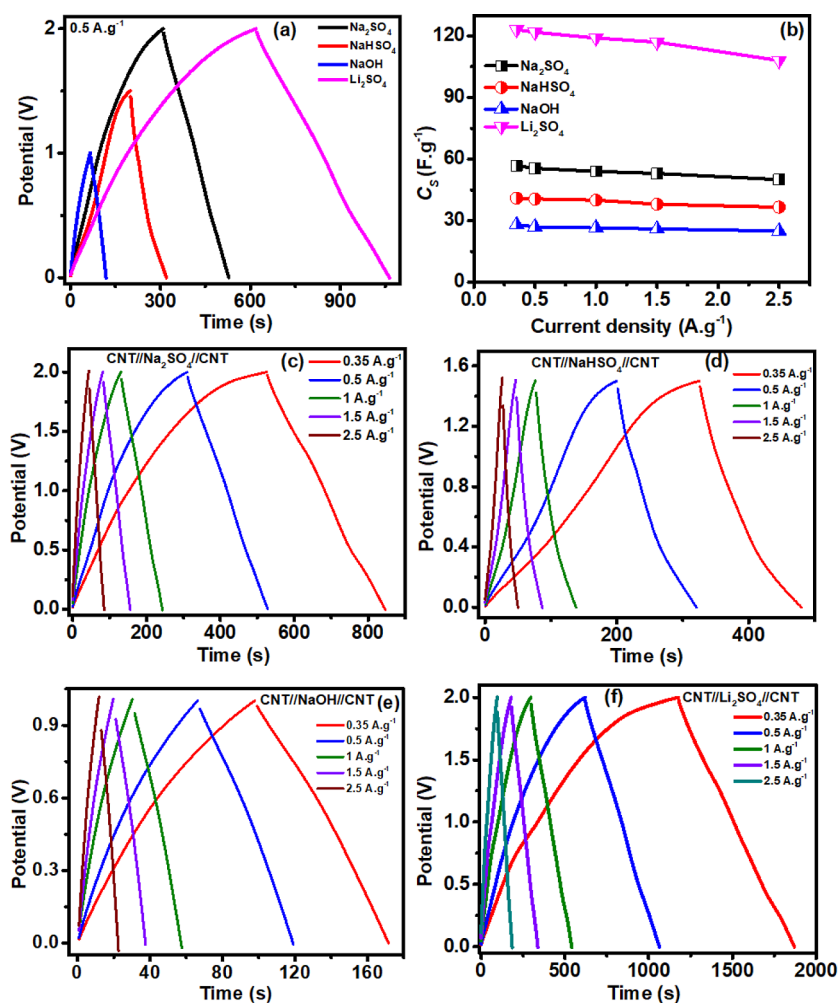

Figure 5. (a) Comparison of GCD curves of CNT//Na$_2$SO$_4$//CNT, CNT//NaHSO$_4$//CNT, CNT//NaOH//CNT, and CNT//Li$_2$SO$_4$//CNT full devices at 0.5 A·g^{-1}. (b) Calculated C_S values for CNT//Na$_2$SO$_4$//CNT, CNT//NaHSO$_4$//CNT, CNT//NaOH//CNT, and CNT//Li$_2$SO$_4$//CNT full devices at various current densities. (c−f) GCD graphs of CNT//Na$_2$SO$_4$//CNT, CNT//NaHSO$_4$//CNT, CNT//NaOH//CNT, and CNT//Li$_2$SO$_4$//CNT full devices at various current densities.

The order of hydrated anionic and cationic radius is SO$_4^{2-}$−H$_2$O > OH$^-$−H$_2$O > HSO$_4^-$−H$_2$O and Li$^+$−H$_2$O > Na$^+$−

H$_2$O. It can also be clearly noticed that the lithium cation and the sulfate anion have larger hydrated sphere radius due to

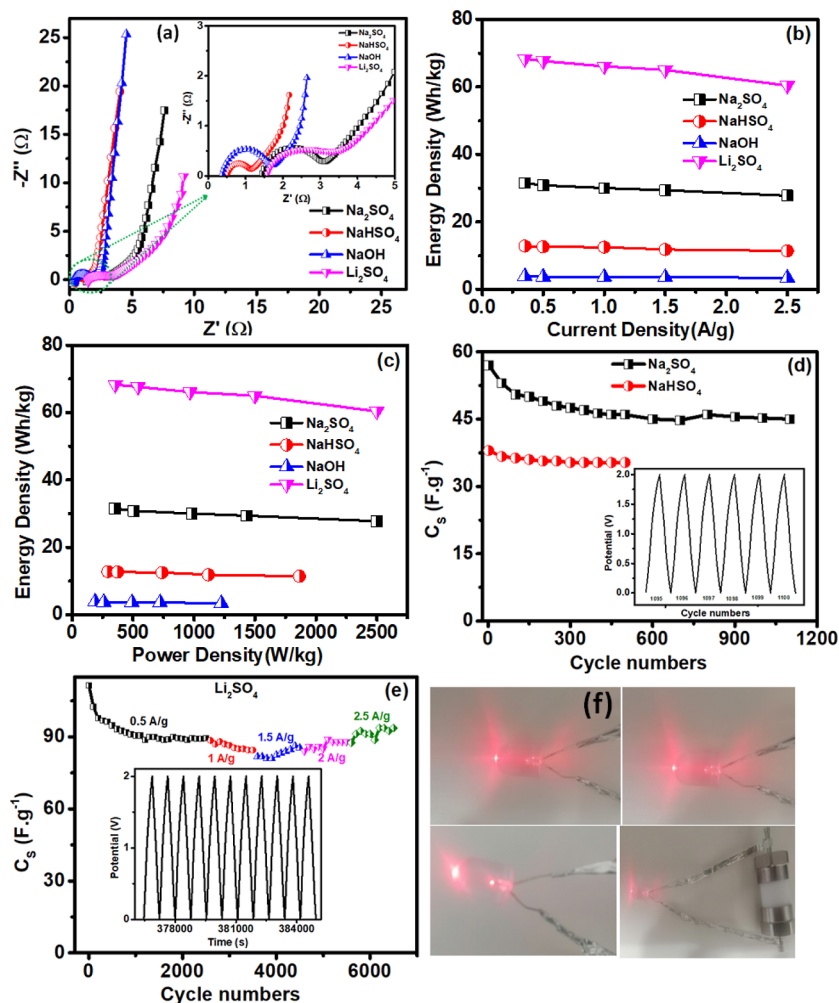**Figure 6.** (a) Comparison of EIS of CNT//Na$_2$SO$_4$//CNT, CNT//NaHSO$_4$//CNT, CNT//NaOH//CNT, and CNT//Li$_2$SO$_4$//CNT full devices. (b) Energy density of CNT//Na$_2$SO$_4$//CNT, CNT//NaHSO$_4$//CNT, CNT//NaOH//CNT, and CNT//Li$_2$SO$_4$//CNT full devices at various current densities. (c) Energy density vs power density of CNT//Na$_2$SO$_4$//CNT, CNT//NaHSO$_4$//CNT, CNT//NaOH//CNT, and CNT//Li$_2$SO$_4$//CNT full devices at various current densities. Calculated C_S values vs number of cycles for (d) CNT//NaHSO$_4$//CNT and CNT//Na$_2$SO$_4$//CNT full devices at 0.5 A·g^{-1}, and (e) CNT//Li$_2$SO$_4$//CNT device at various current densities. (f) Lighting of a 2.1 V, 20 mA, 10 mm red LED by the CNT//Li$_2$SO$_4$//CNT full device after charging at 0.5 A·g^{-1}.

their strong Li$^+$–H$_2$O and SO$_4^{2-}$–H$_2$O interactions caused by the large surface charge density. In EDLCs, simple charging and discharging of the electrical double layer do not need very high ion mobility as compared to pseudocapacitive systems. Once the ions of the electrolyte filled the porous structure of the electrode, the ions already present nearby the interface of the electrolyte/electrode are pushed off and attracted from the electrode on a small distance. Therefore, high mobility might create a problem for efficient and fast charge propagation. The results obtained here in this study proved clearly this assumption as shown in Figure 4a–d. As discussed above, the best results obtained for the CNT//Li$_2$SO$_4$//CNT device might be due to ion dimensions and the potential window. However, it is rather difficult to accurately define the number of water molecules around the anions and cations. The highest capacitance values obtained for the biggest and most solvated cations and anions, that is, Li$^+$ and SO$_4^{2-}$ being surrounded by more water molecules, might be explained by their poor mobility and low diffusion coefficient. As discussed earlier, they remain near the electrode/electrolyte interface during discharging and then quickly appear at this interface during charging as shown in Figure 4a,b. Higher mobilities and

diffusion coefficients describe both HSO$_4^-$ and OH$^-$ anions; consequently, they can migrate into the electrolyte bulk during discharging, and their return to the electrode/electrolyte interface during charging might not be so fast. The same trend can be seen for cations (Li$^+$ and Na$^+$) as shown in Figure 4c,d, although they have the same anion but different cations; therefore, CNT//Li$_2$SO$_4$//CNT showed enhanced electrochemical performance than CNT//Na$_2$SO$_4$//CNT.

The charge/discharge studies further confirmed the excellent electrochemical behavior of the CNT//Li$_2$SO$_4$//CNT device as displayed in Figure 5a–f. Figure 5a shows the comparison of GCD curves for CNT//Li$_2$SO$_4$//CNT, CNT//Na$_2$SO$_4$//CNT, CNT//NaHSO$_4$//CNT, and CNT//NaOH//CNT devices. The shape of the GCD curves is triangular due to their EDLC-type charge storage mechanism present in carbon-based materials. The CNT//Li$_2$SO$_4$//CNT device showed a higher C_S value (~122 F·g^{-1} at 0.5 A·g^{-1}) than CNT//Na$_2$SO$_4$//CNT, CNT//NaHSO$_4$//CNT, and CNT//NaOH//CNT devices (C_S = ~55, ~40, and ~27 F·g^{-1} at 0.5 A g^{-1}). The reason for the higher C_S value for the CNT//Li$_2$SO$_4$//CNT device is already discussed in Figure 4a–d, also due to the porous structure of CNTs, which provide
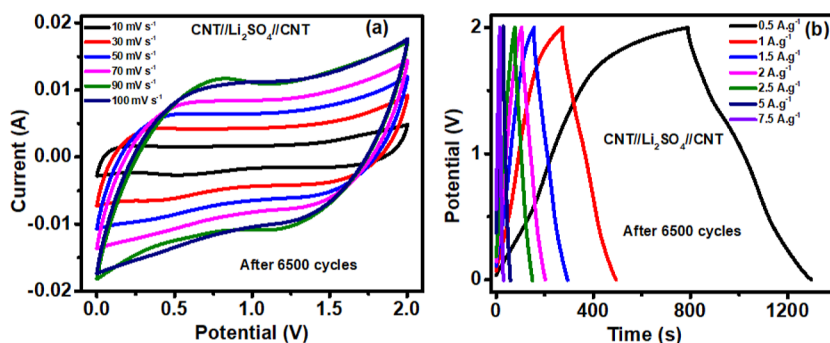
Figure 7. (a,b) CV and GCD graphs for CNT//Li$_2$SO$_4$//CNT full device after 6500 cycles.

more space for ion accumulation at the time of charging. With the increase in current density, the specific capacitance decreases as displayed in Figure 5b and Table S2 for all four devices. Additionally, Figure 5c−f shows the GCD behavior for all the four devices at various current densities.

EIS measurement was performed to study the electrode/electrolyte (electrical resistance and charge transfer resistance) interface at a frequency of 100 mHz to 100 kHz with an amplitude of 5 mV as shown in Figure 6a. The Warburg impedance and Nyquist plots help to understand the electrode's interfacial resistance. Generally, lower charge-transfer resistance and good electrical conductivity are identified by the smaller diameter of the semicircle.[46] The CNT//NaOH//CNT and CNT/NaHSO$_4$//CNT devices showed a smaller semicircle than the other two devices, as shown in the insets of Figure 6a. The CNT//NaOH//CNT and CNT//NaHSO$_4$//CNT devices also have low equivalent series resistance (∼0.2 Ω and 0.5 Ω) than CNT//Na$_2$SO$_4$//CNT and CNT//Li$_2$SO$_4$//CNT devices (∼1.5 and ∼1.6 Ω), which overall denotes the electronic and ionic resistances. The CNT//NaHSO$_4$//CNT and CNT//NaOH//CNT devices also have lower R_{CT} values (∼1.3 and ∼1.7 Ω) than CNT//Na$_2$SO$_4$//CNT and CNT//Li$_2$SO$_4$//CNT devices (∼3.1 and ∼3.4 Ω) because the acidic and basic electrolytes have higher ionic conductivity than neutral electrolytes due to the complete and fast dissociation of ions in solvents.[47]

The potential application of an electrochemical capacitor is further analyzed by the energy and power densities of the device. The energy and power densities of all the devices were calculated by eqs 3 and 4 as given in the Supporting Information. Figure 6b displays the comparison of energy density versus current density graphs for all the four devices. The CNT//Li$_2$SO$_4$//CNT device showed a higher energy density (∼67 W h·kg^{-1} at 0.5 A·g^{-1}) than the CNT//Na$_2$SO$_4$//CNT, CNT//NaHSO$_4$//CNT, and CNT//NaOH//CNT devices (∼30, ∼13, and ∼4 W h·kg^{-1} at 0.5 A·g^{-1}), and the energy density decreases with the increase in current density as shown in Figure 6b for all the four devices. The achieved energy densities are far better than the energy densities reported in the literature. As can be seen from Table S3, the assembled electrochemical capacitor has shown good energy densities with various current densities. Figure 6c displays the comparison graph for the energy and power densities for all the four devices, where the energy densities decrease with the increase in power densities. The CNT//Li$_2$SO$_4$//CNT device showed high energy and power densities than CNT//Na$_2$SO$_4$//CNT, CNT//NaHSO$_4$//CNT, and CNT//NaOH//CNT devices.

In addition to high energy and power densities,[48] a stable and long life cycle is also very crucial for a superior electrochemical capacitor. The cycling stability is a vital factor to analyze the performance of energy storage devices. At a potential window of 0−2 and 0−1.5 V, the cycle stability of the CNT//Li$_2$SO$_4$//CNT device is measured at various current densities (0.5−2.5 A·g^{-1}) for 6500 cycles, and CNT//Na$_2$SO$_4$//CNT and CNT//NaHSO$_4$//CNT devices are measured at 0.5 A·g^{-1} for 1100 and 500 cycles, respectively. As illustrated in Figure 6e, the CNT//Li$_2$SO$_4$//CNT device possesses an initial capacitance of ∼122 F·g^{-1} and maintains ∼115 F·g^{-1} after 6500 cycles at 0.5 A·g^{-1} (ca. 95% of capacitance retention), whereas the CNT//Na$_2$SO$_4$//CNT device possesses an initial capacitance of 55.5 F·g^{-1} and maintains 48.85 F·g^{-1} after 1100 cycles at 0.5 A·g^{-1} (ca. 91.5% of capacitance retention). An increase in specific capacitance from 1.5 to 2.5 A·g^{-1} compared to 1 A·g^{-1} could be due to the electrode−electrolyte stabilization and activation of more pores during the charge−discharge process as shown in Figure 6e.[49] Figure 6d illustrates that the CNT//NaHSO$_4$//CNT device possesses an initial capacitance of 40.6 F·g^{-1} and maintains 35.85 F·g^{-1} after 500 cycles at 1 A·g^{-1} (ca. 96.5% of capacitance retention), denoting outstanding cycle stability too. Remarkably, investigation of the electrochemical stability of the full device at a higher current density of 2.5 A·g^{-1} showed that the CNT//Li$_2$SO$_4$//CNT device has excellent potential for higher energy storage application in the studied potential window. The lighting of a 2.1 V, 20 mA, 10 mm red LED by CNT//Li$_2$SO$_4$//CNT and CNT//Na$_2$SO$_4$//CNT devices after charging at 0.5 A·g^{-1} for more than 2 min is shown in Figure 6f. The CNT//NaHSO$_4$//CNT and CNT//NaOH//CNT devices are not able to light up the LED because of their low operational voltage widow, which is 1.5 and 1 V. The CV and GCD graphs at various scan rates and current densities for the CNT//Li$_2$SO$_4$//CNT device after 6500 cycles are shown in Figure 7a,b. Even after the stability test, all the devices showed the same trend for electrochemical behavior, which confirms the good stability of the device even after higher current densities. The specific capacitance decreases with the increase in scan rate and current density as shown in Figure 7a,b. At a lower scan rate (0.5 A·g^{-1}), the device showed lower overpotential (higher charging time as compared to discharging time) as can be seen in Figure 7b, which may be due to the slight impairment in the structure of CNTs or the electrode−electrolyte destabilization after 6500 cycles. In addition, slight changes in the shape of CV curve have also been noticed after the stability test as displayed in Figure 7a.

4. CONCLUSIONS

In summary, we demonstrated the charge storage mechanism of binder-free electrochemical capacitors in aqueous electrolytes. The physicochemical properties of ions (such as mobility/diffusion and solvation) and their impact on the electrochemical capacitor behavior have been studied. The $CNT//Li_2SO_4//CNT$ device showed excellent electrochemical performance than the other three devices. The reason attributes to the fact that the simple charging and discharging of the electrical double layer in EDLCs do not need very high ion mobility. The ions already present at the electrode/electrolyte interface are attracted to and pushed off from the electrode at a short distance when the electrolyte well saturates on porous electrodes. Hence, high mobility might aggravate fast and efficient charge propagation. The results obtained here in this study proved clearly this assumption as shown in Figure 4a−d. The charge stored by the anions and cations follows the sequence $SO_4^{2-} > HSO_4^- > OH^-$ and $Li^+ > Na^+$. The $CNT//Li_2SO_4//CNT$ device with an operating voltage of 0−2 V exhibits an excellent rate performance with a capacitance retention of 95% at 0.5 A·g^{-1} after 6500 cycles as compared to acidic and basic electrolytes. The neutral medium seems to be a quite fascinating electrolyte solution for electrochemical capacitors. The electrochemical capacitor was also able to light up a red LED (2.1 V) for more than 2 min. However, the present conclusions are based on a single electrode type (CNT); more studies employing electrodes of different chemistry and surface properties are required to draw a complete picture.

■ ASSOCIATED CONTENT

Ⓢ Supporting Information

The Supporting Information is available free of charge at https://pubs.acs.org/doi/10.1021/acsomega.2c07143.

> High-resolution XPS spectra, BET measurement results (including pore distribution and adsorption−desorption isotherms), charge−discharge graphs, and specific capacitance, energy and power densities at various scan rates, and current densities (PDF)

■ AUTHOR INFORMATION

Corresponding Authors

Bhupender Pal − *Department of Inorganic Chemistry, University of Chemistry and Technology Prague, 166 28 Prague, Czech Republic*; Email: palh@vscht.cz

Zdeněk Sofer − *Department of Inorganic Chemistry, University of Chemistry and Technology Prague, 166 28 Prague, Czech Republic*; ⓞ orcid.org/0000-0002-1391-4448; Email: zdenek.sofer@vscht.cz

Authors

Kalyan Jyoti Sarkar − *Department of Inorganic Chemistry, University of Chemistry and Technology Prague, 166 28 Prague, Czech Republic*

Bing Wu − *Department of Inorganic Chemistry, University of Chemistry and Technology Prague, 166 28 Prague, Czech Republic*

Lukáš Děkanovský − *Department of Inorganic Chemistry, University of Chemistry and Technology Prague, 166 28 Prague, Czech Republic*

Vlastimil Mazánek − *Department of Inorganic Chemistry, University of Chemistry and Technology Prague, 166 28 Prague, Czech Republic*

Rajan Jose − *Center for Advanced Intelligent Materials Technology and Faculty of Industrial Sciences & Technology, Universiti Malaysia Pahang, Kuantan 26300, Malaysia*; ⓞ orcid.org/0000-0003-4540-321X

Complete contact information is available at:
https://pubs.acs.org/10.1021/acsomega.2c07143

Notes

The authors declare no competing financial interest.

■ ACKNOWLEDGMENTS

■ REFERENCES

(1) Liu, C.-F.; Liu, Y.-C.; Yi, T.-Y.; Hu, C.-C. Carbon materials for high-voltage supercapacitors. *Carbon* **2019**, *145*, 529−548.

(2) Gopi, C. V. M.; Vinodh, R.; Sambasivam, S.; Obaidat, I. M.; Kim, H.-J. Recent progress of advanced energy storage materials for flexible and wearable supercapacitor: From design and development to applications. *J. Energy Storage.* **2020**, *27*, 101035.

(3) Béguin, F.; Presser, V.; Balducci, A.; Frackowiak, E. Carbons and electrolytes for advanced supercapacitors. *Adv. Mater.* **2014**, *26*, 2219−2283.

(4) Simon, P.; Gogotsi, Y. Perspectives for electrochemical capacitors and related devices. *Nat. Mater.* **2020**, *19*, 1151−1163.

(5) Simon, P.; Gogotsi, Y. Materials for electrochemical capacitors. *Nat. Mater.* **2008**, *7*, 845−854.

(6) Weinstein, L.; Dash, R. Supercapacitor carbons. *Mater. Today.* **2013**, *10*, 356−357.

(7) Hashempour, M.; Vicenzo, A.; Bahdanchyk, M.; Bestetti, M. Parameters influencing the capacitive behavior of carbon composite electrodes: composition, morphology, electrical conductivity, and surface chemistry. *J. Solid State Electrochem.* **2018**, *22*, 3895−3911.

(8) Han, J.; Kim, W.; Kim, H.-K.; Youn, H.-C.; Han, J. T.; Kim, W.; Roh, K. C. Longitudinal unzipped carbon nanotubes with high specific surface area and trimodal pore structure. *RSC Adv.* **2016**, *6*, 8661−8668.

(9) Borenstein, A.; Hanna, O.; Attias, R.; Luski, S.; Brousse, T.; Aurbach, D. Carbon-based composite materials for supercapacitor electrodes: a review. *J. Mater. Chem. A* **2017**, *5*, 12653−12672.

(10) Pan, H.; Li, J.; Feng, Y. Carbon nanotubes for supercapacitor. *Nanoscale Res. Lett.* **2010**, *5*, 654−668.

(11) Xu, K. Nonaqueous liquid electrolytes for lithium-based rechargeable batteries. *Chem. Rev.* **2004**, *104*, 4303−4418.

(12) Pal, B.; Yang, S.; Ramesh, S.; Thangadurai, V.; Jose, R. Electrolyte selection for supercapacitive devices: A critical review. *Nanoscale Adv.* **2019**, *1*, 3807−3835.

(13) Zhong, C.; Deng, Y.; Hu, W.; Qiao, J.; Zhang, L.; Zhang, J. A review of electrolyte materials and compositions for electrochemical supercapacitors. *Chem. Soc. Rev.* **2015**, *44*, 7484−7539.

(14) Wu, H.; Wang, X.; Jiang, L.; Wu, C.; Zhao, Q.; Liu, X.; Hu, L.; Yi, L. The effects of electrolyte on the supercapacitive performance of activated calcium carbide-derived carbon. *J. Power Sources* **2013**, *226*, 202−209.

(15) Liu, P.; Verbrugge, M.; Soukiazian, S. Influence of temperature and electrolyte on the performance of activated-carbon supercapacitors. *J. Power Sources* **2006**, *156*, 712−718.

(16) Mun, Y.; Jo, C.; Hyeon, T.; Lee, J.; Ha, K.-S.; Jun, K.-W.; Lee, S.-H.; Hong, S.-W.; Lee, H. I.; Yoon, S.; Lee, J. Simple synthesis of hierarchically structured partially graphitized carbon by emulsion/block-copolymer co-template method for high power supercapacitors. *Carbon* **2013**, *64*, 391−402.

(17) Jin, Z.; Yan, X.; Yu, Y.; Zhao, G. Sustainable activated carbon fibers from liquefied wood with controllable porosity for high-performance supercapacitors. *J. Mater. Chem. A* **2014**, *2*, 11706−11715.

(18) Bichat, M.; Raymundo-Piñero, E.; Béguin, F. High voltage supercapacitor built with seaweed carbons in neutral aqueous electrolyte. *Carbon* **2010**, *48*, 4351−4361.

(19) Pal, B.; Yasin, A.; Kunwar, R.; Yang, S.; Yusoff, M. M.; Jose, R. Polymer versus cation of gel polymer electrolytes in the charge storage of asymmetric supercapacitors. *Ind. Eng. Chem. Res.* **2018**, *58*, 654−664.

(20) Brandt, A.; Isken, P.; Lex-Balducci, A.; Balducci, A. Adiponitrile-based electrochemical double layer capacitor. *J. Power Sources* **2012**, *204*, 213−219.

(21) Qu, Q.; Wang, B.; Yang, L.; Shi, Y.; Tian, S.; Wu, Y. Study on electrochemical performance of activated carbon in aqueous Li_2SO_4, Na_2SO_4 and K_2SO_4 electrolytes. *Electrochem. Commun.* **2008**, *10*, 1652−1655.

(22) Yang, Z.; Tian, J.; Yin, Z.; Cui, C.; Qian, W.; Wei, F. Carbon nanotube-and graphene-based nanomaterials and applications in high-voltage supercapacitor: A review. *Carbon* **2019**, *141*, 467−480.

(23) Zang, X.; Shen, C.; Sanghadasa, M.; Lin, L. High-voltage supercapacitors based on aqueous electrolytes. *ChemElectroChem* **2019**, *6*, 976−988.

(24) Aldama, I.; Barranco, V.; Kunowsky, M.; Ibañez, J.; Rojo, J. M. Contribution of cations and anions of aqueous electrolytes to the charge stored at the electric electrolyte/electrode interface of carbon-based supercapacitors. *J. Phys. Chem. C* **2017**, *121*, 12053−12062.

(25) Zhu, J.; Xu, Y.; Wang, J.; Lin, J.; Sun, X.; Mao, S. The effect of various electrolyte cations on electrochemical performance of polypyrrole/RGO based supercapacitors. *Phys. Chem. Chem. Phys.* **2015**, *17*, 28666−28673.

(26) Yang, H.; Yang, J.; Bo, Z.; Chen, X.; Shuai, X.; Kong, J.; Yan, J.; Cen, K. Kinetic-dominated charging mechanism within representative aqueous electrolyte-based electric double-layer capacitors. *J. Phys. Chem. Lett.* **2017**, *8*, 3703−3710.

(27) Cheng, C.; Uhe, J.; Yang, X.; Wu, Y.; Li, D. Multilayered graphene membrane as an experimental platform to probe nano-confined electrosorption. *Prog. Nat. Sci.: Mater. Int.* **2012**, *22*, 668−672.

(28) Kaempgen, M.; Ma, J.; Gruner, G.; Wee, G.; Mhaisalkar, S. Bifunctional carbon nanotube networks for supercapacitors. *Appl. Phys. Lett.* **2007**, *90*, 264104.

(29) Niu, Z.; Zhou, W.; Chen, J.; Feng, G.; Li, H.; Ma, W.; Li, J.; Dong, H.; Ren, Y.; Zhao, D.; Xie, S. Compact-designed super-capacitors using free-standing single-walled carbon nanotube films. *Energy Environ. Sci.* **2011**, *4*, 1440−1446.

(30) Masarapu, C.; Zeng, H. F.; Hung, K. H.; Wei, B. Effect of temperature on the capacitance of carbon nanotube supercapacitors. *ACS Nano* **2009**, *3*, 2199−2206.

(31) Li, P.; Kong, C.; Shang, Y.; Shi, E.; Yu, Y.; Qian, W.; Wei, F.; Wei, J.; Wang, K.; Zhu, H.; Cao, A.; Wu, D. Highly deformation-tolerant carbon nanotube sponges as supercapacitor electrodes. *Nanoscale* **2013**, *5*, 8472−8479.

(32) Zheng, C.; Qian, W.; Cui, C.; Zhang, Q.; Jin, Y.; Zhao, M.; Tan, P.; Wei, F. Hierarchical carbon nanotube membrane with high packing density and tunable porous structure for high voltage supercapacitors. *Carbon* **2012**, *50*, 5167−5175.

(33) Yuksel, R.; Sarioba, Z.; Cirpan, A.; Hiralal, P.; Unalan, H. E. Transparent and flexible supercapacitors with single walled carbon nanotube thin film electrodes. *ACS Appl. Mater. Interfaces* **2014**, *6*, 15434−15439.

(34) Kaempgen, M.; Chan, C. K.; Ma, J.; Cui, Y.; Gruner, G. Printable thin film supercapacitors using single-walled carbon nanotubes. *Nano Lett.* **2009**, *9*, 1872−1876.

(35) Yu, C.; Masarapu, C.; Rong, J.; Wei, B.; Jiang, H. Stretchable supercapacitors based on buckled single-walled carbon-nanotube macrofilms. *Adv. Mater.* **2009**, *21*, 4793−4797.

(36) Niu, Z.; Dong, H.; Zhu, B.; Li, J.; Hng, H. H.; Zhou, W.; Chen, X.; Xie, S. Highly stretchable, integrated supercapacitors based on single-walled carbon nanotube films with continuous reticulate architecture. *Adv. Mater.* **2013**, *25*, 1058−1064.

(37) Li, X.; Gu, T.; Wei, B. Dynamic and galvanic stability of stretchable supercapacitors. *Nano Lett.* **2012**, *12*, 6366−6371.

(38) Niu, Z.; Zhou, W.; Chen, J.; Feng, G.; Li, H.; Hu, Y.; Ma, W.; Dong, H.; Li, J.; Xie, S. A repeated halving approach to fabricate ultrathin single-walled carbon nanotube films for transparent supercapacitors. *Small* **2013**, *9*, 518−524.

(39) Lee, J.; Kim, W.; Kim, W. Stretchable carbon nanotube/ion−gel supercapacitors with high durability realized through interfacial microroughness. *ACS Appl. Mater. Interfaces* **2014**, *6*, 13578−13586.

(40) Zong, S.; Du, J.; Chen, A.; Gao, X.; Otun, K. O.; Liu, X.; Jewell, L. L. Compounds. N-doped crumpled carbon nanotubes as advanced electrode material for supercapacitor. *J. Alloys Compd.* **2022**, *928*, 167222.

(41) Zhu, S.; Chang, Y.; Hou, W.; Li, Y.; Ni, J.; Han, G. Molten-salt directed mesopore engineering of carbon nanotubes for energetic quasi-solid-state supercapacitors. *Carbon* **2022**, *200*, 75−83.

(42) Shi, L.; Yang, W.; Zha, X.; Zeng, Q.; Tu, D.; Li, Y.; Yang, Y.; Xu, J.; Chen, F. Metal-organic frameworks-derived porous carbon nanotube for high performance supercapacitor electrode materials. *Colloids Surf. A* **2022**, *652*, 129862.

(43) Qi, H.; Schulz, B. r.; Vad, T.; Liu, J.; Mäder, E.; Seide, G.; Gries, T. Novel carbon nanotube/cellulose composite fibers as multifunctional materials. *ACS Appl. Mater. Interfaces* **2015**, *7*, 22404−22412.

(44) Avendano, C.; Brun, N.; Fontaine, O.; In, M.; Mehdi, A.; Stocco, A.; Vioux, A. Multiwalled carbon nanotube/cellulose composite: from aqueous dispersions to pickering emulsions. *Langmuir* **2016**, *32*, 3907−3916.

(45) Marcus, Y. A simple empirical model describing the thermodynamics of hydration of ions of widely varying charges, sizes, and shapes. *Biophys. Chem.* **1994**, *51*, 111−127.

(46) Chung, D. Y.; Lee, K. J.; Yu, S. H.; Kim, M.; Lee, S. Y.; Kim, O. H.; Park, H. J.; Sung, Y. E. Alveoli-inspired facile transport structure of N-doped porous carbon for electrochemical energy applications. *Adv. Energy Mater.* **2015**, *5*, 1401309.

(47) Pal, B.; Yasin, A.; Kaur, R.; Tebyetekerwa, M.; Zabihi, F.; Yang, S.; Yang, C.-C.; Sofer, Z.; Jose, R. Understanding electrochemical capacitors with in-situ techniques. *Renew. Sustain. Energy Rev.* **2021**, *149*, 111418.

(48) Bo, Z.; Yi, K.; Yang, H.; Guo, X.; Huang, Z.; Zheng, Z.; Yan, J.; Cen, K.; Ostrikov, K. K. More from less but precise: Industry-relevant pseudocapacitance by atomically-precise mass-loading MnO_2 within multifunctional MXene aerogel. *J. Power Sources* **2021**, *492*, 229639.

(49) Krishnan, G. S.; Reddy, M. V.; Harilal, M.; Vidyadharan, B.; Misnon, I. I.; Rahim, H. M.; Ismail, J.; Jose, R. Characterization of $MgCo_2O_4$ as an electrode for high performance supercapacitors. *Electrochim. Acta* **2015**, *161*, 312−321.